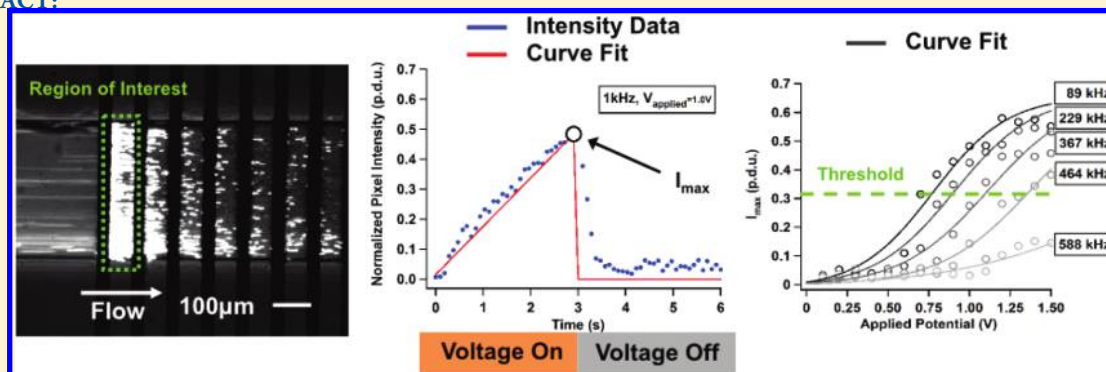


# Automated Dielectrophoretic Characterization of *Mycobacterium smegmatis*

Benjamin G. Hawkins,<sup>†</sup> Chao Huang,<sup>†</sup> Srinitya Arasanipalai,<sup>‡</sup> and Brian J. Kirby<sup>\*,‡</sup>

<sup>†</sup>Department of Biomedical Engineering, and <sup>‡</sup>Sibley School of Mechanical and Aerospace Engineering, Cornell University, Ithaca, New York, United States

## ABSTRACT:



We report the positive dielectrophoretic (pDEP) characterization of wild-type and ethambutol-treated *Mycobacterium smegmatis* populations via automated pDEP cell trapping experiments. The automated technique was validated by measurements of carboxylate-modified polystyrene microspheres and *Escherichia coli*. The characterization of *M. smegmatis* identifies a key frequency regime where the membrane-specific action of ethambutol leads to a change in the cellular dielectrophoretic response. This work represents the first such characterization of *Mycobacteria* and highlights the potential for DEP measurements to measure changes in mycobacterial membrane properties associated with chemical treatments or genetic mutation.

Dielectrophoresis (DEP) is the transport of polarizable particles in response to a nonuniform electric field, exclusive of electrophoresis.<sup>1</sup> DEP forces depend on the magnitude and nonuniformity of an externally applied electric field, as well as the complex permittivity of a particle and its surrounding media.<sup>2</sup> The complex permittivities of the particle and surrounding media are a function of the frequency of the polarizing electric field, electrical conductivity, and permittivity. Material permittivity values constitute an instantaneous approximation of the medium response and are, thus, generally a function of the electric field frequency, depending on the orientational, atomic, and electronic polarizabilities.<sup>3</sup> Over the range of frequencies considered in this work, however, these effects are negligible and the permittivity,  $\epsilon$ , is assumed independent of frequency. The combination of material and frequency dependence makes DEP a useful technique for researchers attempting to manipulate, separate, and characterize particles and cells.

In this work, we present an automated DEP-based characterization technique and apply it to the bacterial species *Mycobacterium smegmatis*. *M. smegmatis* is a nonpathogenic, acid-fast, Gram-positive bacteria with a membrane structure similar to other, pathogenic species such as *M. tuberculosis*. The outer layer of *M. smegmatis* is composed of covalently attached lipids, namely  $\alpha$ -, keto-, and methoxy-mycolic acids. Some

*Mycobacteria* additionally possess a pseudocapsule of noncovalently attached lipids. Mycolic acids, specifically the complex trehalose dimycolate in *M. tuberculosis*, are responsible for the host inflammatory and granulomatous responses<sup>4,5</sup> that are the primary symptoms of tuberculosis infection. In addition to their adjuvant effects on the host immune system, the lipid content of mycobacterial species forms a dense, hydrophobic barrier to antibiotics, contributing to mycobacterial drug resistance. These membrane lipids are bound to the polysaccharide arabinogalactan.<sup>6</sup> The antimycobacterial drug ethambutol inhibits biosynthesis of arabinogalactan, limiting mycolate attachment sites and significantly altering membrane composition.<sup>7</sup> Due to its role in pathogenicity and host immune response, the exterior lipid composition of the cell membrane of mycobacterial species is relevant to studies of membrane biosynthesis, drug resistance, and pathogenicity.

DEP devices have been used to characterize and separate a variety of species, e.g., bacterial populations,<sup>8–11</sup> mammalian cells,<sup>12–15</sup> DNA,<sup>16</sup> proteins,<sup>17–20</sup> and viruses.<sup>21</sup> Indeed, DEP devices have been used to identify surface monolayer and membrane properties of particles and cells, respectively.<sup>22,23</sup>

Received: January 24, 2011

Accepted: March 10, 2011

Published: April 04, 2011

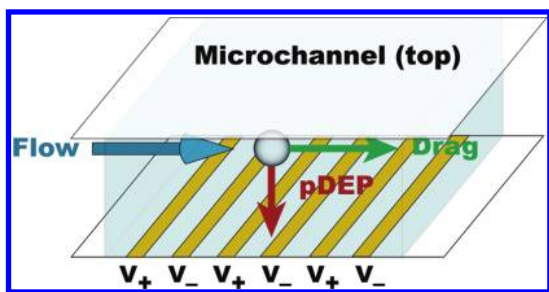


**Figure 1.** Interdigitated electrode array configured with alternating positive ( $V_+$ ) and negative ( $V_-$ ) electrodes on the bottom of a microfluidic channel. Fluid drag moves particles with the direction of flow while pDEP forces attract particles to the electrode array. Negative DEP forces repel particles from the array.

DEP separation techniques are often binary, centering on the crossover frequency, at which the sign of the DEP force changes. For samples with different crossover frequencies, there exists a frequency regime where the DEP force is positive for one population and negative for another. Another class of DEP-based separation techniques depend on differences in the magnitude of the DEP force at a particular frequency.<sup>8,11,24,25</sup> Because the crossover frequency can be insensitive to changes in cell membrane composition (the primary component affected by ethambutol), it is beneficial to investigate separation techniques that depend on the magnitude of the DEP force. These separation techniques require characterization of cellular dielectric response as a function of frequency to determine the optimal regime for efficient operation.

## THEORY

We use a combination of numerical and analytical techniques to model particle behavior near an interdigitated electrode array. The configuration of the array and the direction of positive DEP forces are shown in Figure 1.

**Dielectrophoresis and Cell Modeling.** We start by considering a sphere in an infinite domain with homogeneous and isotropic complex permittivities. In a uniform field  $\mathbf{E} = \mathbf{E}_0 \cos(\omega t)$ , the contribution of a polarized sphere to the total electric field can be described by an electric dipole with a moment,<sup>2,3,26</sup>  $\mathbf{p} = \mathbf{p}_0(\cos \omega t + \varphi)$ :

$$\mathbf{p}_0 = 4\pi\epsilon_m a^3 \left[ \frac{\tilde{\epsilon}_p - \tilde{\epsilon}_m}{\tilde{\epsilon}_p + 2\tilde{\epsilon}_m} \right] \mathbf{E}_0 \quad (1)$$

where  $a$  is the particle radius,  $\mathbf{E}$  is the externally applied electric field, and the subscripts  $m$  and  $p$  refer to the medium and particle, respectively.  $\tilde{\epsilon} = \epsilon - i\sigma/\omega$  is the complex permittivity,  $\epsilon$  is the permittivity,  $\sigma$  is the electrical conductivity,  $\omega$  is the frequency of the applied electric field (in rad/s), and  $i = (-1)^{1/2}$ . If the field is slightly nonuniform over the length scale of the particle, then the force on the dipole will be  $\mathbf{F} = \mathbf{p} \cdot \nabla \mathbf{E}$ . Assuming no net free charge, this yields the following expression for the time-averaged dielectrophoretic force:<sup>2</sup>  $\langle \mathbf{F}_{\text{DEP}} \rangle = \pi a^3 \mathcal{R}(\tilde{f}_{\text{CM}}) \nabla(\mathbf{E}_0 \cdot \mathbf{E}_0)$ .

For ellipsoidal particles (specifically, a prolate spheroid), a change of variables can be performed, and a similar analytical

solution can be found<sup>2,27</sup> for particles oriented with their long axis parallel to the external electric field (along the  $z$  axis):

$$\langle \mathbf{F}_{\text{DEP},z} \rangle = \pi\epsilon_m l_z l_x l_y^2 \mathcal{R} \left[ \frac{\tilde{\epsilon}_p - \tilde{\epsilon}_m}{3[\tilde{\epsilon}_m + (\tilde{\epsilon}_p - \tilde{\epsilon}_m)L_z]} \right] \nabla(\mathbf{E}_0 \cdot \mathbf{E}_0) \quad (2)$$

where  $l_z$  and  $l_x (= l_y)$  are the lengths of the major and minor axes, respectively.  $L_z$  is the “depolarizing factor” along the major axis:

$$L_z = \frac{l_{x,y}^2}{2l_z^2 e^3} \left[ \ln \left( \frac{1+e}{1-e} \right) - 2e \right] \quad (3)$$

where  $e = (1 - l_{x,y}^2/l_z^2)^{1/2}$  is the particle eccentricity.

To describe particles with inhomogeneous complex permittivity such as cells, a multishell model is often invoked, using spherically symmetric layers of constant thickness, permittivity, and conductivity.<sup>28–30</sup> Using the same change of variables, an ellipsoidal particle can also be described with the multishell approach, if the shells can be approximated as confocal. Although this is typically not exact for cells, the ellipsoidal multishell model provides a convenient analytical tool to describe coccolidal bacteria. A prolate spheroid with a single shell of complex permittivity,  $\tilde{\epsilon}_s$ , has a dipole coefficient (analogous to  $\tilde{f}_{\text{CM}}$  for spherical particles):

$$\tilde{K}_{z,1} = \frac{\tilde{\epsilon}_p - \tilde{\epsilon}_m}{3[\tilde{\epsilon}_m + L_1(\tilde{\epsilon}_s - \tilde{\epsilon}_m)] + 9\tilde{K}_{z,0}\gamma L_1(1-L_1)(\tilde{\epsilon}_s - \tilde{\epsilon}_m)} \quad (4)$$

where  $\gamma$  is the ratio of volumes of the core to the whole spheroid and  $\tilde{K}_{z,0}$  is the spheroidal complex Clausius–Mossotti factor:

$$\tilde{K}_{z,0} = \frac{\tilde{\epsilon}_p - \tilde{\epsilon}_s}{3[\tilde{\epsilon}_s + L_1(\tilde{\epsilon}_p - \tilde{\epsilon}_s)]} \quad (5)$$

Additional shells can be added as described by Castellarnau et al.<sup>11</sup> and Huang et al.,<sup>31</sup> with the  $n$ -shell factor described as

$$\tilde{K}_{z,n} = \frac{1}{3} \frac{(\tilde{\epsilon}_m - \tilde{\epsilon}_{n-1}) + 3\tilde{K}_{z,n-1}x_{n-1}(\tilde{\epsilon}_{n-1} + L_{z,n}(\tilde{\epsilon}_m - \tilde{\epsilon}_{n-1}))}{(\tilde{\epsilon}_m + L_{z,n}(\tilde{\epsilon}_{n-1} - \tilde{\epsilon}_m)) + 3\tilde{K}_{z,n-1}x_{n-1}L_{z,n}(1-L_{z,n})(\tilde{\epsilon}_{n-1} - \tilde{\epsilon}_m)} \quad (6)$$

$$x_n = \frac{(hl_{x,y} + \sum_{k=1}^{n-1} \delta_k)(l_{x,y} + \sum_{k=1}^{n-1} \delta_k)^2}{(hl_{x,y} + \sum_{k=1}^n \delta_k)(l_{x,y} + \sum_{k=1}^n \delta_k)^2} \quad (7)$$

$$L_{z,n} = \frac{1 - e_n^2}{2e_n^3} \left[ \log \left( \frac{1+e_n}{1-e_n} \right) - 2e_n \right] \quad (8)$$

$$e_n = \sqrt{1 - \left( \frac{l_{x,y} + \sum_{k=1}^n \delta_k}{hl_{x,y} + \sum_{k=1}^n \delta_k} \right)^2} \quad (9)$$

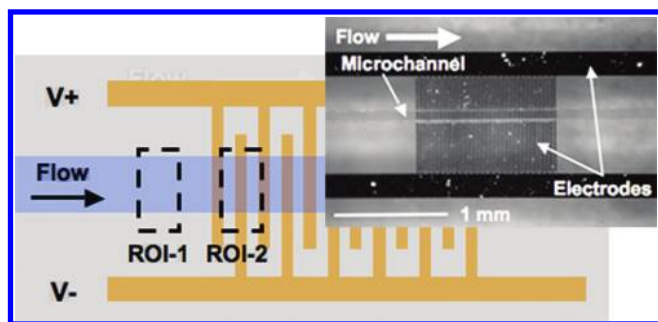


**Figure 2.** Interdigitated electrode array schematic with regions of interest (ROI-1 and ROI-2) defined. The average pixel intensity in ROI-1 was used as a background intensity signal proportional to particle density and fluorescence staining intensity. The average pixel intensity in ROI-2 was used as a measure of particle trapping. Inset shows a top view of the fabricated device with PDMS channel.

where  $h = l_z/l_{x,y}$  is the particle spheroid aspect ratio ( $h > 1$  for a prolate spheroid) and  $\delta_n$  refers to the thickness of the  $n$ th shell. In an effort to account for some of the error induced by the confocal shell approximation, specifically that incurred due to varying shell thicknesses, eqs 7 and 9 redefine the volume ratio,  $x_n$ , and eccentricity,  $e_n$ , to exclude the aspect ratio,  $h$ , from the shell thickness parameter,  $\delta_n$ .

In this study, a three-shell model ( $n = 5$ ) was used to approximate the structure and composition of bacterial samples. This model accounts for the complex permittivity and relative sizes of the cytoplasm ( $n = 1$ ), cytoplasmic membrane ( $n = 2$ ), cell wall ( $n = 3$ ), and media ( $n = 5$ ). The outer shell ( $n = 4$ ) of the particle was used to approximate the outer membrane in *E. coli* samples and the covalently bound lipids in *M. smegmatis* samples.

The homogeneous sphere model for polystyrene in water neglects the significant surface conductance that dominates the particle response at low frequency. It has been shown by several researchers that carboxylate-modified polystyrene microspheres exhibit a significant surface conductance that contributes to particle dielectrophoretic behavior.<sup>33–35,40,41</sup> Polystyrene microspheres are therefore modeled as a homogeneous particle with a surface conductance that contributes significantly to the effective particle conductivity:<sup>32–35</sup>

$$\sigma_p = \sigma_{p,\text{bulk}} + 2\frac{K_s}{a} \quad (10)$$

where  $\sigma_{p,\text{bulk}}$  is the bulk particle conductivity and  $K_s$  is the surface conductance.

**Electric Field and Cell Collection Modeling.** The DEP force is a direct function of the electrical properties of the particle and the fluid medium (related by the real part of the Clausius–Mossotti factor,  $\mathcal{R}[\tilde{f}_{\text{CM}}]$ ), as well as the magnitude and frequency of the applied electric field. To characterize the DEP response of particles and cells, we fabricated a device with a microchannel defined in poly(dimethylsiloxane) (PDMS) and bonded on top of gold interdigitated electrodes deposited on glass (Figure 2, inset). In certain ranges of electric field magnitude and frequency, the positive DEP force acting on a particle will overcome fluid drag and trap the particle onto the electrodes. The intensity of trapped, fluorescently labeled particles was recorded over time and was fit to a series of physically informed functions such that a quantitative measure of particle trapping, a “threshold trapping potential”, can be defined and compared

between trials and samples. This trapping potential data is inversely proportional to the square root of  $\mathcal{R}[\tilde{f}_{\text{CM}}]$  and allows for the relative magnitudes of the particles’ DEP responses to be measured.

The electric field above a pair of interdigitated electrodes can be approximated by assuming that the gap between the electrodes is differentially small. The resulting expressions for the electric field and the dielectrophoretic force on a homogeneous spherical particle are<sup>8,36</sup>

$$\mathbf{E} = \frac{V}{\pi r} \hat{\theta} \quad (11)$$

$$\langle \mathbf{F}_{\text{DEP}} \rangle = \frac{a^3 \epsilon_m}{3\pi r^3} \mathcal{R}[\tilde{f}_{\text{CM}}] V^2 \hat{r} \quad (12)$$

where  $\hat{\theta}$  and  $\hat{r}$  are unit vectors in cylindrical coordinates,  $r$  is the radial distance from the center of the electrode gap, and  $V$  is the applied potential.

Following the analysis of Sanchis et al.,<sup>8</sup> we assume that particles reach terminal velocity instantaneously and that particle trapping occurs in a stagnant fluid. Under these conditions, we can calculate the time required to trap a particle on the electrode array from a distance  $r_{\text{trap}}$  from the electrode gap. The resulting relationship gives the approximate number of cells,  $N$ , on the array after a time,  $\Delta t$ , given a cell number density,  $n_0$ .  $r_{\text{trap}}$  defines a trapping horizon that expands as  $\Delta t$  increases. During the time,  $\Delta t$ ,  $N$  cells within a semicylindrical volume swept by  $r_{\text{trap}}$  are trapped on the array.

$$N \approx n_0 \frac{\pi r_{\text{trap}}^2 w}{2} \approx \frac{n_0 w a V}{6} \sqrt{\frac{2\epsilon_m \mathcal{R}[\tilde{f}_{\text{CM}}] \Delta t}{\eta}} \quad (13)$$

where  $w$  is the channel width (length of electrode) and  $\eta$  is the fluid viscosity. The addition of a pressure-driven (Poiseuille) flow profile will transform (scale and shear) the trapping horizon but is not expected to significantly alter the scaling relationship between  $N$  and the applied potential,  $V$ . We can rearrange this relationship to express  $\tilde{f}_{\text{CM}}$  as a function of the trapping potential,  $V_{\text{trapping}}$ :

$$\mathcal{R}[\tilde{f}_{\text{CM}}] \sim \frac{\eta}{n_0^2 w^2 a^2 \epsilon_m} \frac{N^2}{\Delta t} \frac{1}{V_{\text{trapping}}^2} \quad (14)$$

The number density and trapping time,  $\Delta t$ , are fixed parameters in the experiment, so the number of cells collected is a function of  $\mathcal{R}[\tilde{f}_{\text{CM}}]$ . Rather than measuring the number of captured cells, as done in other DEP collection experiments,<sup>8,14</sup> we measure the potential,  $V_{\text{trapping}}$ , required to trap a particular number (or, more precisely, number density) of cells in a region of interest.  $V_{\text{trapping}}$  is defined by a threshold value of the maximum fluorescence intensity,  $I_{\text{max}}$ , discussed in the next section. By defining  $V_{\text{trapping}}$  as the potential where the measured fluorescence intensity is  $I_{\text{max}}/2$ , we account for experiment-to-experiment variations in particle concentration.

**Data Collection and Analysis.** Here we describe the theoretical aspects of our data collection and analysis procedure, specifically the definition of  $V_{\text{trapping}}$  and  $I_{\text{max}}$  in terms of experimental data. An automated data collection scheme was developed to measure particle trapping as a function of electric field frequency and magnitude (electric field parameters vary and are discussed later in Materials and Methods). A custom LabVIEW interface controlled the electric field inputs of the experiment—

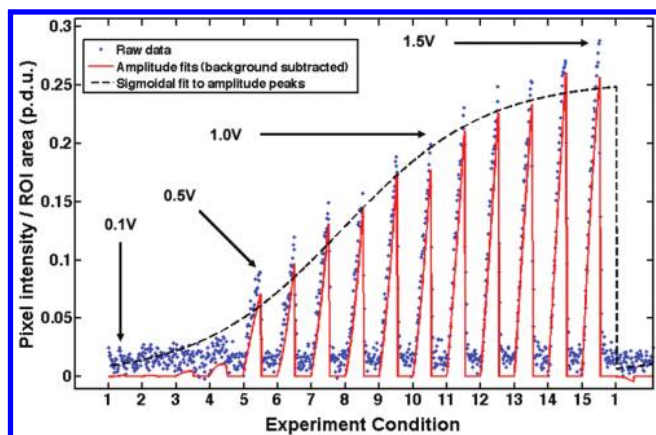


**Figure 3.** Raw average pixel intensity data from ROI-2 (blue points) was fit to quadratic curves (solid red) at each “experiment condition”—corresponding to a particular frequency—potential pair. In this example data set, taken at 1 kHz with polystyrene beads, experimental conditions 1–15 correspond to applied potentials of 0.1–1.5 V in 0.1 V increments. The peaks of each quadratic fit were fit to a sigmoid (dashed black) whose plateau was determined by the maximum measured average pixel intensity for all frequency–potential pairs in an experiment.

magnitude, frequency, “on” duration, and “off” duration—and recorded the fluorescence intensity outputs. Fluorescence intensity was integrated over a region of interest and normalized by the number of pixels to give an average pixel intensity. The average pixel intensity is then a function of the magnitude of the DEP force, which in turn depends on particle composition and on electric field magnitude and frequency. Inflow particle density was assumed uniform and constant throughout all experiments. Variations in particle fluorescence intensity were controlled by careful staining protocols and corrected for during data analysis by comparing trapping data to bulk sample concentration.

The spatially averaged pixel intensity was recorded over the course of the experiment for two separate regions of interest: upstream of the electrode array (ROI-1) and around the gaps between the first, second, and third electrodes (ROI-2, Figure 2). ROI-1 was used as a representative measure of bulk sample concentration to account for changes in particle number density. ROI-2 measured the intensity of particles trapped on the array. The order in which frequencies were applied was randomized for every experiment. Three experiments were performed for every trial, and for biological samples, each trial was a separately cultured and prepared sample.

To quantitatively compare sample DEP response, a series of analyses were performed in MATLAB to account for background fluorescence, particle density fluctuations, and permanent particle adhesion to the electrodes. Data from each experiment was broken down into subsets containing data for a particular frequency. Within each frequency subset, we identify “experiment conditions” corresponding to a particular frequency–potential pair. Data for each experiment condition is a time series of normalized pixel intensity data within each ROI with the electric field on then off. To account for variations in particle solution concentration, the bulk particle concentration signal (ROI-1) was subtracted from the particle trapping signal (ROI-2) for the entire experimental data set. Next, “off-time” data from each experimental condition was smoothed by a locally weighted scatterplot smoothing function, and the minimum of this smoothed curve was subtracted from the experiment condition data; this step

accounts for permanent particle adhesion over the course of the experiment. Next, “on-time” data from each experimental condition was fit to a quadratic curve which served as a low-pass filter for measurement noise (Figure 3). The “on-time” and “off-time” analyses were performed over all experimental conditions within each data subset (i.e., for each frequency), and the maximum quadratic fit for the entire experiment (i.e., over all potentials and frequencies) was recorded as  $I_{\max}$ . Finally, for each data subset, the peaks of the quadratic curves were fit to a sigmoidal curve with a peak plateau region set to  $I_{\max}$ .

$$I_{\text{fit}} = \frac{I_{\max}}{1 + \frac{e^{-nx}}{b}} \quad (15)$$

Identifying a unique value of  $I_{\max}$  for each (experimental) data set corrected for experimental variability due to particle concentration variations or electrode surface contamination between experiments. A sigmoidal fit was chosen because it characterizes the trapping behavior of particles well, including a lower region before trapping is observed and a saturation region as the trapped particles fill the space near the electrodes. If the goodness of the sigmoidal fit did not exceed a defined threshold ( $R^2 > 0.7$ ), then the data subset from that particular applied frequency was excluded. In almost all cases, data subsets for which  $R^2 < 0.7$  occurred at frequencies where  $\langle F_{\text{DEP}} \rangle$  is expected to be low or negative and no particles trapped in the region of interest.

The threshold trapping potential,  $V_{\text{trapping}}$  for each applied frequency was defined as the voltage at which the sigmoidal fit function at that frequency has a value of  $I_{\max}/2$ ; for frequencies at which DEP forces are weak, this gives values larger than the experimental voltage range, with increased uncertainty associated with the extrapolation of the data. The trapping potential as a function of frequency was obtained for polystyrene particles or bacteria in solutions of varying conductivity. The inverse square of the trapping potential was calculated to compare the relative DEP response magnitudes of the particles and cells.

## MATERIALS AND METHODS

**Device Fabrication.** Electrodes were fabricated by use of standard lift-off photolithography. Four inch borofloat glass wafers were cleaned with hot piranha solution and vapor-primed with HMDS. Microposit S1818 photoresist was spun onto the wafers at 3000 rpm for 30 s and baked at 115 °C for 60 s. Photoresist was exposed with an EV620 contact aligner in soft-contact mode for 2 s ( $12 \text{ mW}/\text{cm}^2$ ). Photoresist was developed in Microposit MF-321 for 120 s. Wafers were then treated for 90 s with oxygen plasma to descum and then placed in a CVC SC4500 electron-beam evaporator. A 200 nm layer of gold was deposited between 50 nm and 10 nm layers of chrome. Lift-off was performed in a Microposit Remover 1165 for 12 h. Wafers were then coated with resist and diced (K&S 7100 dicing saw).

Fluid channel fabrication was accomplished by use of standard soft lithography. First, a silicon master was fabricated with 25  $\mu\text{m}$  tall features by use of standard photolithography. Wafers were coated with Microposit S1818 photoresist (3000 rpm, 30 s) and exposed for 2 s ( $12 \text{ mW}/\text{cm}^2$ ). Features were etched to a depth of 25  $\mu\text{m}$  with a Unaxis 770 Bosch reactive ion etch tool and resist-stripped with reactive oxygen plasma (Gasonics Aura 1000). Wafers were coated with 1H,1H,2H,2H-perfluorooctyltrichlorosilane (FOTS) by use of a vacuum evaporation process to prevent

PDMS adhesion. PDMS monomer and curing agent were mixed in a 15:1 ratio for 5 min and placed under vacuum to remove bubbles. The PDMS mixture was then poured over the silicon master in a custom-made jig and placed in an oven to cure for 12 h at 60 °C. PDMS devices were cut to size, and via holes were created with a biopsy punch. PDMS channels and electrode devices were cleaned in an air plasma at 250 mTorr vacuum for 45 s (Harrick Plasma) and immediately bonded. Electrodes were connected externally to wires with silver conductive epoxy.

**Sample Preparation.** Lyophilized *E. coli* (K-12 wild-type, EMG 2: K ( $\lambda$ ), ATCC 23716, passage 1–2) and *M. smegmatis* (mc(2)155, ATCC 700084, passage 1–2) samples were obtained from ATCC. Cultures were grown in LB media (*E. coli*) and Middlebrook 7H9 media with OADC enrichment (100 mL/L) (*M. smegmatis*), respectively. Media solutions were obtained from Becton/Dickinson and prepared as directed by the manufacturer, with the exception of using OADC enrichment in Middlebrook 7H9 media. *E. coli* cells were grown in liquid media (10 mL of LB broth) in an incubating shaker at 37 °C and 350 rpm for 24 h. *E. coli* were then plated in Petri dishes on LB agar (prepared as directed by the manufacturer) and incubated for 24 h at 37 °C. *M. smegmatis* cells were grown under the same conditions in liquid media (10 mL of Middlebrook 7H9) for 48 h. *M. smegmatis* cells were then plated on LB agar with 0.5 mL/L Tween 80 and incubated for 48 h at 37 °C. Petri dishes were then sealed with paraffin, inverted, and refrigerated.

*E. coli* cells were taken from first or second passage solid culture and placed in 10 mL of LB media in sterile 14 mL polystyrene culture tubes (loosely capped). Samples were allowed to grow through log phase to stationary phase (18–24 h) before preparation. *M. smegmatis* samples were prepared identically with the exception of culture media (Middlebrook 7H9 with OADC enrichment) and growth time to stationary phase (36–48 h). Cells were grown to stationary phase—as determined by representative growth rate experiments, optical density ( $OD_{650}$ ) measurements (data not shown), and data available in literature<sup>37</sup>—prior to preparation. To assess the impact of cell membrane composition on DEP response, samples of *M. smegmatis* were treated with ethambutol (ETB) at a concentration of 10  $\mu$ g/mL after 24 h of growth, and the treatment was maintained at this concentration throughout preparation and experiment. Growth in liquid culture was carried out in an incubating shaker at 37 °C at 350 rpm. Samples of 1 mL were removed and placed in centrifuge tubes and spun down at 5000g for 10 min. The samples were resuspended in 0.85% (w/v) NaCl in deionized water and allowed to incubate for 1 h. Samples were then spun down again and resuspended in 0.85% (w/v) NaCl with 4  $\mu$ L/mL of BACLIGHT live/dead stain (Molecular Probes) and allowed to incubate in the dark (culture oven, 37 °C) for 1 h. The samples were then washed once with and then resuspended in 0.5% (w/v) Tween 80 solution (a subset of *E. coli* samples were processed in DI water for comparison). *M. smegmatis* samples were analyzed to confirm that treatment with ethambutol did not meaningfully affect fluorescence intensity or cell size. A representative sample was evaluated with Phylum analysis software for cell length and diameter as well as average intensity. Wild-type and ethambutol-treated samples exhibited lengths of 1.24 and 1.33  $\mu$ m with standard deviations of 0.14 and 0.11  $\mu$ m, respectively. Average pixel intensity per cell was 1037 p.d.u. (WT) and 1041 p.d.u. (ETB) with standard deviations of 49.9 and 45.1, respectively.

Fluoresbrite 1.75  $\mu$ m diameter carboxylate-modified polystyrene microspheres (beads) were obtained from Polysciences, Inc.

Beads were spun down at 5000g for 10 min and resuspended in DI water with trace amounts of salt (KCl) to control conductivity. Particles were diluted to a density of  $\sim 4.25 \times 10^6$  particles/mL in polystyrene bead samples.

**Data Acquisition and Processing.** Prepared samples were drawn into a Hamilton Gastight 1000 1 mL glass syringe (Hamilton Company, U.S.A.) and dispensed at a rate of 10  $\mu$ L/h by a Chemyx Fusion 400 syringe pump. The precision glass syringe and high step resolution of the syringe pump (0.02  $\mu$ m) combined to significantly reduce variability in the volumetric flow rate. The syringe was coupled to the PDMS channel with a 30 gauge needle and Tygon microbore tubing (o.d., 0.76 mm; i.d., 0.25 mm). Electric potentials were applied to the electrode array by an Agilent 33200A arbitrary waveform generator and controlled with a custom LabVIEW interface (National Instruments Corporation, U.S.A.).

The LabVIEW interface controlled the electric field frequency, magnitude, “on” time, and “off” time. The “on” time was fixed at 3 s for all experiments, and the “off” time was 3 s for polystyrene bead samples and 5 s for biological samples. Electric field frequencies (40 points, logarithmically spaced between 1 kHz and 10 MHz) were ordered randomly in each experiment and tested at every potential. Potentials were applied, in order, from 0.1 to 1.5 V in 0.1 V increments (2.5 V in 0.2 V increments in ethambutol-treated *M. smegmatis* experiments) to minimize electrode fouling over the course of the experiment.

Particle trapping was measured with a Nikon LV100 upright microscope with long working distance objectives (Nikon S Plan Fluor, 40 $\times$ /0.60, 3.6–2.8 mm), a EXFO X-Cite series 120 fluorescence excitation source, and a QImaging EXiFast Blue high-speed monochrome CCD camera.

**Safety.** Electrical components present a shock hazard. Disconnect electrical power while making connections and take proper safety precautions when energizing electrical components. Biological specimens and toxic chemicals (e.g., ethambutol) should be handled with care. Appropriate personal protective equipment should be worn at all times and disposed of properly.

## RESULTS AND DISCUSSION

**Polystyrene Microspheres.** Carboxylate-modified polystyrene microspheres were tested in solutions with three different conductivities (adjusted by addition of KCl) to show that, as expected, trapping potential increases in the low-frequency regime as media conductivity increases. This is consistent with a decrease in  $\mathcal{R}[f_{CM}]$  over the same frequency range. The apparent crossover frequency is  $\sim 10^6$  Hz, decreasing with increasing conductivity in Figure 4, parts a and b.

The data in Figure 4b were fit to eq 10 by use of a nonlinear least-squares method in MATLAB. Fits shown in Figure 4b were calculated using the constants listed in Table 1 with  $C_0$  and  $K_s$  as free parameters.  $C_0$  is a scaling constant related to flow conditions and electrode geometry. Fixed parameter values were set to exact values, whereas free parameters were constrained to physically reasonable values inferred from previously published data.<sup>33–35,41</sup> Low-conductivity data was well-fit by a simple surface conductivity model (eq 10) with the parameters listed in Table 1. However, as conductivity increased, the model becomes less appropriate, as evidenced by decreasing values of  $R^2$ . The values obtained for surface conductance are similar to those proposed by Green and Morgan<sup>33</sup> and Hughes and Morgan.<sup>35</sup> The crossover frequency

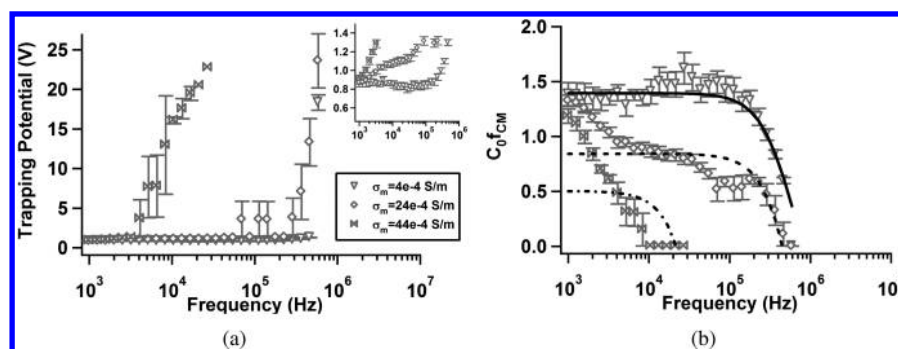


**Figure 4.** Trapping potential,  $V_{\text{trapping}}$  (a) and  $C_0 \mathcal{R}[\tilde{f}_{\text{CM}}] (= 1/V_{\text{trapping}}^2)$  (b) as a function of frequency for  $1.75 \mu\text{m}$  diameter carboxylate-modified polystyrene particles suspended in aqueous solutions with conductivities  $\sigma_m = 4 \times 10^{-4}$ ,  $\sigma_m = 24 \times 10^{-4}$ , and  $\sigma_m = 44 \times 10^{-4}$ . Inset in panel a expands the low-potential range for clarity. Inset axes are the same as panel a:  $V_{\text{trapping}}$  (ordinate) and frequency (abscissa). Curve fits in panel b were calculated with an effective surface conductance model (eq 10). Error bars represent standard error of the mean:  $S_e = S_d/(n)^{1/2}$  where  $S_d$  is the standard deviation. The symbol  $C_0$  denotes an arbitrary constant related to the flow rate and electrode geometry.

**Table 1.** Multivariable Fit Coefficients Chosen to Match Experimental Measurements of the Real Part of the Clausius–Mossotti Factor,  $\mathcal{R}[\tilde{f}_{\text{CM}}]$ , for Carboxylate-Modified Polystyrene Particles in Solutions of Increasing Conductivity<sup>a</sup>

parameter	$\sigma_m = 0.4 \text{ mS/m}$	$\sigma_m = 2.4 \text{ mS/m}$	$\sigma_m = 4.4 \text{ mS/m}$
	Fixed		
$\epsilon_p$	2.5	2.5	2.5
$\epsilon_m$	78.5	78.5	78.5
$\sigma_p$	$1 \times 10^{-12} \text{ S/m}$	$1 \times 10^{-12} \text{ S/m}$	$1 \times 10^{-12} \text{ S/m}$
$r$	$0.876 \times 10^{-6} \text{ m}$	$0.876 \times 10^{-6} \text{ m}$	$0.876 \times 10^{-6} \text{ m}$
	Free		
$K_s$	$2.13 \times 10^{-9} \text{ S}$	$1.5 \times 10^{-9} \text{ S}$	$1.9 \times 10^{-9} \text{ S}$
$C_0$	1.33	2.71	70.7
$R^2$	0.942	0.417	0.11

<sup>a</sup> Parameters are divided into fixed (above) and free (below) groups. Fixed parameters and limits of free parameters were based on previously published data (refs 33–35, 41).

predicted by a homogeneous-particle model remains constant at low medium conductivity ( $< \sim 1 \times 10^{-3}$ ), then decreases rapidly and disappears when  $\tilde{\epsilon}_m > \tilde{\epsilon}_p$ .<sup>33</sup> The experimentally observed decrease in crossover frequency with increasing conductivity is often attributed to surface conductance and double layer polarization effects.<sup>33</sup> Recent work by Basuray and co-workers has managed to capture this change in crossover frequency by considering polarization and ion transport within the double layer.<sup>38,39</sup>

***E. coli*.** As additional verification of our experimental data collection and data analysis techniques, we measured the pDEP response of *E. coli* in DI water and 0.5% (w/v) Tween 80 solution. The results, Figure 5, show a constant trapping potential for low frequency which then increases above  $10^5$  Hz and peaks near  $10^6$  Hz before decreasing again. This is consistent with our model predictions for *E. coli* as well as experimental results obtained by Sanchis et al.<sup>8</sup> and Castellarnau et al.<sup>11</sup>

The data were well-fit by the spheroidal three-shell model discussed previously (i.e., eq 6). To obtain these fits, two rounds of fitting were performed. Initial fits for *E. coli* in DI water were performed, allowing all parameters to vary while constrained by values obtained in the literature.<sup>8,11</sup> After initial fitting, cytoplasmic, plasma membrane, and cell wall coefficients were fixed along with outer membrane conductivity, and data for *E. coli* in 0.5%

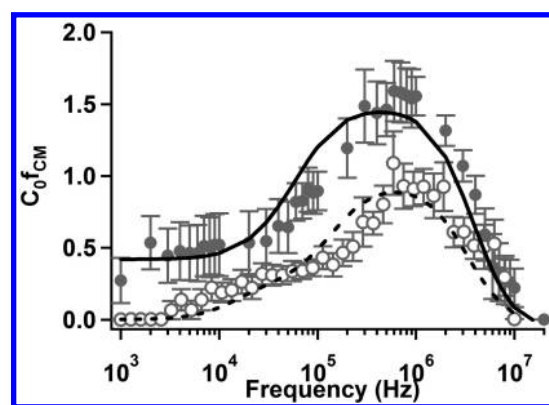


**Figure 5.**  $C_0 \mathcal{R}[\tilde{f}_{\text{CM}}] (= 1/V_{\text{trapping}}^2)$  as a function of frequency for wild-type *E. coli* suspended in DI water (filled circles,  $\sigma_m \approx 0.05 \text{ mS/m}$ ) and 0.5% (w/v) Tween 80 solution (open circles,  $\sigma_m \approx 1 \text{ mS/m}$ ). Curve fits for *E. coli* in DI water (solid) and 0.5% (w/v) Tween 80 solution (dashed) were calculated using a multivariate nonlinear least-squares technique to a spheroidal multishell model. Error bars represent standard error of the mean. The symbol  $C_0$  denotes an arbitrary constant related to the flow rate and electrode geometry.

(w/v) Tween 80 were fit as before, allowing the permittivity of the outer membrane to vary. The results of fitting are given in Table 2. In the presence of 0.5% (w/v) Tween, the outer membrane permittivity increased by a factor of 3. Although by no means conclusive, this result suggests that the presence of the surfactant in solution may have interacted with the outer membrane and contributed to the local effective permittivity.

***M. smegmatis*.** *M. smegmatis* is a Gram-positive bacterium with both a different shape and different composition from *E. coli*. We therefore expect a different trapping response owing to the presence of the lipid/mycolic acid region of the mycobacterial envelope. Indeed, we do observe such a distinction, particularly below  $\sim 10^6$  Hz where *E. coli* samples exhibit significant low-frequency dispersion that is not observed in *M. smegmatis*. This low-frequency component to the DEP response is indicative of multiple Maxwell–Wagner relaxation frequencies, which can result when the interfaces between materials are not well-defined. At still lower frequencies (i.e.,  $1 \times 10^4$  Hz) the so-called  $\alpha$ -relaxation associated with ion motion within the double layer is one potential explanation for the observed pDEP response.<sup>33,42–44</sup>

**Table 2. Multivariable Fit Coefficients for the Clausius–Mossotti Factor,  $\mathcal{R}[\tilde{K}_z]$ , for *E. coli* in Deionized Water and a 0.5% (w/v) Solution of Tween 80 (Figure 5)<sup>a</sup>**

parameter	DI water	0.5% (w/v) Tween 80
	Fixed	
$\epsilon_m$	78.5	78.5
$\epsilon_{\text{cyto}}$	60	60
$\epsilon_{\text{pmem}}$	2.3	2.3
$\epsilon_{\text{wall}}$	60	60
$\sigma_m$	$5 \times 10^{-5}$ S/m	$1 \times 10^{-3}$ S/m
$\sigma_{\text{cyto}}$	0.1 S/m	0.1 S/m
$\sigma_{\text{pmem}}$	$6 \times 10^{-6}$ S/m	$6 \times 10^{-6}$ S/m
$\sigma_{\text{wall}}$	$1.9 \times 10^{-4}$ S/m	$1.9 \times 10^{-4}$ S/m
$\sigma_{\text{mem}}$	$2.2 \times 10^{-6}$ S/m	$2.2 \times 10^{-6}$ S/m
$r$	$0.5 \times 10^{-6}$ m	$0.5 \times 10^{-6}$ m
$\delta_{\text{pmem}}$	$8 \times 10^{-9}$ m	$8 \times 10^{-9}$ m
$\delta_{\text{wall}}$	$15 \times 10^{-9}$ m	$15 \times 10^{-9}$ m
$\delta_{\text{mem}}$	$8 \times 10^{-9}$ m	$8 \times 10^{-9}$ m
	Free	
$\epsilon_{\text{mem}}$	2	6.3
$C_0$	0.99	0.517
$R^2$	0.90	0.8075

<sup>a</sup>Parameters are divided into fixed (above) and free (below) groups. Fixed parameters and limits of free parameters were based on previously published data (refs 8 and 11).

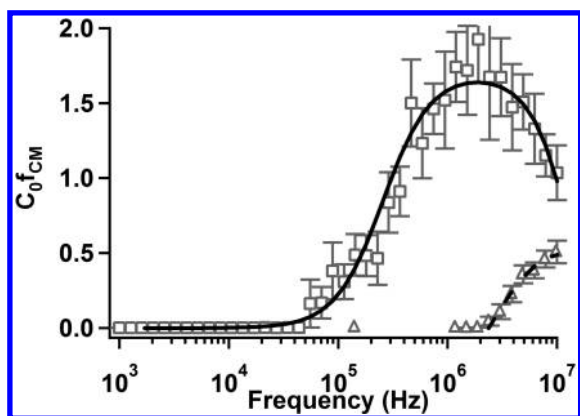


**Figure 6.**  $C_0 \mathcal{R}[\tilde{f}_{\text{CM}}] (= 1/V_{\text{trapping}}^2)$  as a function of frequency for wild-type (open squares) and ethambutol-treated (open triangles) *M. smegmatis* suspended in 0.5% (w/v) Tween 80 solution ( $\sigma_m \approx 1$  mS/m). Curve fits for wild-type (solid) and ethambutol-treated (dashed) samples were calculated using a multivariate nonlinear least-squares technique to a spheroidal multishell model. Error bars represent standard error of the mean. The symbol  $C_0$  denotes an arbitrary constant related to the flow rate and electrode geometry.

Treatment with ethambutol significantly alters the dielectrophoretic response of *M. smegmatis*. *Mycobacteria* are susceptible to modification of their membrane composition using ethambutol to inhibit the production of arabinogalactan and prevent the attachment of mycolic acids. The removal of the outer layer of lipids exposes the peptidoglycan<sup>6,45</sup> and significantly decreases the effective permittivity of the cell. Treatment with ethambutol caused the values of  $1/V_{\text{trapping}}^2$  to be significantly diminished

**Table 3. Multivariable Fit Coefficients for the Clausius–Mossotti Factor,  $\mathcal{R}[\tilde{K}_z]$ , for Wild-Type and Ethambutol-Treated *M. smegmatis* in a 0.5% (w/v) Solution of Tween 80 (Figure 6)<sup>a</sup>**

parameter	WT <i>M. smegmatis</i>	ETB-treated <i>M. smegmatis</i>
	Fixed	
$\epsilon_m$	78.5	78.5
$\epsilon_{\text{cyto}}$	70	70
$\sigma_m$	$1 \times 10^{-3}$ S/m	$1 \times 10^{-3}$ S/m
$r$	$0.3 \times 10^{-6}$ m	$0.3 \times 10^{-6}$ m
$\delta_{\text{pmem}}$	$7 \times 10^{-9}$ m	$7 \times 10^{-9}$ m
$\delta_{\text{mem}}$	$40 \times 10^{-9}$ m	$40 \times 10^{-9}$ m
	Free	
$\epsilon_{\text{pmem}}$	5.65	2
$\epsilon_{\text{wall}}$	13	3
$\epsilon_{\text{lipid}}$	10.5	78.5
$\sigma_{\text{cyto}}$	0.3 S/m	0.98 S/m
$\sigma_{\text{pmem}}$	$5.5 \times 10^{-5}$ S/m	$2.6 \times 10^{-4}$ S/m
$\sigma_{\text{wall}}$	$1.33 \times 10^{-4}$ S/m	$3.6 \times 10^{-4}$ S/m
$\sigma_{\text{lipid}}$	$1.0 \times 10^{-4}$ S/m	$11.5 \times 10^{-4}$ S/m
$\delta_{\text{lipid}}$	$84 \times 10^{-9}$ m	$53 \times 10^{-9}$ m
$C_0$	9.72	7.68
$R^2$	0.97	0.96

<sup>a</sup>Parameters are divided into fixed (above) and free (below) groups. Fixed parameters and limits for free parameters were based on previously published data (refs 8, 11, 47–50).

and shifted toward higher frequencies ( $\sim 10^6$ – $10^7$  Hz). The dramatic difference observed in Figure 6 confirms the effect that ethambutol has on mycobacterial membrane composition. The data in Figure 6 can be fit by the spheroidal multishell model introduced earlier. Parameters used to generate curve fits are given in Table 3. The aspect ratio,  $h$ , for *M. smegmatis* was 3.3, calculated from measurements by Nguyen et al.<sup>46</sup> Thicknesses were estimated based on the work of Takade et al.<sup>47</sup> and Paul and Beveridge<sup>48–50</sup> or inferred from the curve fit process.

The results of the curve fitting analysis indicate a wide range of changes within the cell membrane as a result of treatment with ethambutol. There are slight variations in the permittivity and conductivity of the plasma membrane and cell wall, and an increase in cytoplasmic conductivity. The most dramatic change, however, occurs in the outer membrane or lipid region, where both the permittivity and conductivity increased to approximately those of the external media. The thickness of the lipid region also decreased. These are both suggestive of the antimycotic acid action of ethambutol, which has been shown to prevent the attachment of mycolic acids in the outer membrane.

Chan et al. examined the accuracy and sensitivity of parameters extracted from electrorotation data (related to DEP trapping data by Kramers–Krönig relationships) by use of a three-shell model.<sup>51</sup> Their results indicate that the accuracy of extracted inner membrane and cytoplasmic parameters decreased as noise in the electrorotation data increased. This indicates that the effects of these material properties are somewhat subtle and difficult to extract relative to parameters such as the outer membrane permittivity. In our analysis, we noticed qualitatively similar behavior when we used unconstrained

parameters; large variations in inner membrane parameters elicited subtle changes, while outer-shell parameters affected gross changes in the resulting fit. As a result, the data obtained in this work reflects changes in a lumped, membrane capacitance parameter. In an attempt to correlate these results with physical changes in cell structure, we refine the lumped parameter model into multiple components (shells). In doing so, we sacrifice the uniqueness of our results but demonstrate consistency with the proposed changes in membrane structure. The key conclusions of this work are that the changes measured in *E. coli* and *M. smegmatis* are consistent with, and suggestive of, changes in the outer membrane structure.

A wide array of techniques are available for characterization of the dielectrophoretic response of a sample. The majority rely on electrorotation<sup>12,31,52–54</sup> or measurements of the crossover frequency.<sup>11</sup> The electrorotation force is largest at the crossover frequency, making measurements in this frequency regime easier, compared to the positive and negative DEP forces, which are vanishingly small approaching the crossover frequency and tend to be larger, and thus easier to measure, far from the crossover frequency.<sup>51,55</sup> The use of DEP “collection spectra” has been employed to characterize a number of different cell types, to screen bacteria for antibiotic resistance, and to detect cancerous cells.<sup>8,14,56,57</sup> By associating fluorescence intensity with collection spectra, we can automate the data collection and analysis process. The resulting quantitative characterization of  $V_{\text{trapping}}$  allows comparison of the magnitude of pDEP forces on a particular sample, a crucial step when developing dielectrophoresis-based sorting techniques that rely on a difference in the magnitude of  $\Re[\tilde{\chi}_{\text{CM}}]$ .

## CONCLUSION

In this work, we present a novel automated experimental technique with which we measured the effects of ethambutol treatment on the positive dielectrophoretic response of *M. smegmatis*. This represents the first such characterization of the dielectrophoretic response of *M. smegmatis*. In addition, experiments were performed to measure the pDEP response of carboxylate-modified polystyrene microspheres and wild-type *E. coli*. Polystyrene bead data were fit with a surface conductance model, and bacterial data were fit with a spheroidal multishell model. The results of this characterization technique garner insight into frequency regimes where membrane-specific differences in mycobacterial cells manifest as significant changes in their dielectrophoretic response.

The automated pDEP characterization of wild-type and ethambutol-treated *M. smegmatis* performed in this study shows that ethambutol significantly alters cell dielectrophoretic response in a manner that is consistent with a removal or permeabilization of the outer lipid structure of these cells. Wild-type (mc(2)155) *M. smegmatis* exhibit pDEP response above  $5 \times 10^4$  Hz, whereas ethambutol-treated bacteria exhibited pDEP response only above  $2 \times 10^7$  Hz. This frequency regime may represent a key frequency space where dielectrophoresis-based sorting techniques can be implemented to measure changes in mycobacterial membrane properties associated with chemical treatments or genetic mutation.

## AUTHOR INFORMATION

### Corresponding Author

\*E-mail: kirby@cornell.edu.

## ACKNOWLEDGMENT

This work is supported by the National Science Foundation, Grant CBET-0828997. B.G.H. and C.H. also acknowledge support from NSF Graduate Research Fellowships.

## REFERENCES

- (1) Pohl, H. A. *Dielectrophoresis: The Behavior of Neutral Matter in Nonuniform Electric Fields*; Cambridge University Press: New York, 1978.
- (2) Jones, T. B. *Electromechanics of Particles*; Cambridge University Press: New York, 1995.
- (3) Morgan, H.; Green, N. G. *AC Electrokinetics: Colloids and Nanoparticles*; Research Studies Press: Hertfordshire, U.K., 2003.
- (4) Rhoades, E. R.; Geisel, R. E.; Butcher, B. A.; McDonough, S.; Russell, D. G. *Tuberculosis (Edinburgh, Scotland)* **2005**, *85*, 159–176.
- (5) Korf, J.; Stoltz, A.; Verschoor, J.; De Baetselier, P.; Grooten, J. *Eur. J. Immunol.* **2005**, *35*, 890–900.
- (6) Alsteens, D.; Verbelen, C.; Dague, E.; Raze, D.; Baulard, A. R.; Dufrene, Y. F. *Pfluegers Arch: Eur. J. Physiol.* **2008**, *456*, 117–125.
- (7) Mikusová, K.; Slayden, R. A.; Besra, G. S.; Brennan, P. J. *Antimicrob. Agents Chemother.* **1995**, *39*, 2484–2489.
- (8) Sanchis, A.; Brown, A. P.; Sancho, M.; Martnez, G.; Sebastián, J. L.; Muñoz, S.; Miranda, J. M. *Bioelectromagnetics* **2007**, *28*, 393–401.
- (9) Lapizco-Encinas, B. H.; Simmons, B. A.; Cummings, E. B.; Fintschenko, Y. *Anal. Chem.* **2004**, *76*, 1571–1579.
- (10) Cho, Y.-K.; Kim, S.; Lee, K.; Park, C.; Lee, J.-G.; Ko, C. *Electrophoresis* **2009**, *30*, 3153–3159.
- (11) Castellarnau, M.; Errachid, A.; Madrid, C.; Juárez, A.; Samitier, J. *Biophys. J.* **2006**, *91*, 3937–3945.
- (12) Yang, J.; Huang, Y.; Wang, X.; Wang, X.-B.; Becker, F. F.; Gascoyne, P. R. C. *Biophys. J.* **1999**, *76*, 3307–3314.
- (13) Yang, J. *Biophys. J.* **2000**, *78*, 2680–2689.
- (14) Gascoyne, P.; Noshari, J.; Becker, F.; Pethig, R. *IEEE Trans. Ind. Appl.* **1994**, *30*, 829–834.
- (15) Das, C. M.; Becker, F.; Vernon, S.; Noshari, J.; Joyce, C.; Gascoyne, P. R. C. *Anal. Chem.* **2005**, *77*, 2708–2719.
- (16) Chou, C. F.; Tegenfeldt, J. O.; Bakajin, O.; Chan, S. S.; Cox, E. C.; Darnton, N.; Duke, T.; Austin, R. H. *Biophys. J.* **2002**, *83*, 2170–2179.
- (17) Clarke, R. W.; White, S. S.; Zhou, D.; Ying, L.; Klenerman, D. *Angew. Chem., Int. Ed.* **2005**, *44*, 3747–3750.
- (18) Clarke, R.; Piper, J.; Ying, L.; Klenerman, D. *Phys. Rev. Lett.* **2007**, *98*, 198102–6.
- (19) Hölzel, R.; Calander, N.; Chiragwandi, Z.; Willander, M.; Bier, F. *Phys. Rev. Lett.* **2005**, *95*, 128102–4.
- (20) Lapizco-Encinas, B. H.; Ozuna-Chacón, S.; Rito-Palomares, M. *J. Chromatogr., A* **2008**, *1206*, 45–51.
- (21) Hughes, M.; Morgan, H.; Rixon, F.; Burt, J.; Pethig, R. *Biochim. Biophys. Acta* **1998**, *1425*, 119–126.
- (22) Vykoukal, J.; Vykoukal, D. M.; Sharma, S.; Becker, F. F.; Gascoyne, P. R. C. *Langmuir* **2003**, *19*, 2425–2433.
- (23) Oblak, J.; Krizaj, D.; Amon, S.; Macek-Lebar, A.; Miklavcic, D. *Bioelectrochemistry* **2007**, *71*, 164–171.
- (24) Das, C. M.; Becker, F.; Vernon, S.; Noshari, J.; Joyce, C.; Gascoyne, P. R. C. *Anal. Chem.* **2005**, *77*, 2708–2719.
- (25) Hawkins, B. G.; Smith, A. E.; Syed, Y. A.; Kirby, B. J. *Anal. Chem.* **2007**, *79*, 7291–7300.
- (26) Kirby, B. J. *Micro- and Nanoscale Fluid Mechanics: Transport in Microfluidic Devices*; Cambridge University Press: New York, 2010.
- (27) Stratton, J. A. *Electromagnetic Theory*; McGraw-Hill: New York, 1941.
- (28) Hughes, M. P.; Morgan, H.; Rixon, F. J.; Burt, J. P.; Pethig, R. *Biochim. Biophys. Acta* **1998**, *1425*, 119–126.
- (29) Froude, V. E.; Zhu, Y. *J. Phys. Chem. B* **2009**, *113*, 1552–1558.
- (30) Korlach, J.; Reichle, C.; Müller, T.; Schnelle, T.; Webb, W. W. *Biophys. J.* **2005**, *89*, 554–562.

- (31) Huang, J. P.; Gu, G. Q.; Karttunen, M. *Phys. Rev. E* **2003**, *67*, 51405.
- (32) Bikerman, J. J. *Trans. Faraday Soc.* **1940**, *35*, 154.
- (33) Green, N. G.; Morgan, H. J. *Phys. Chem. B* **1999**, *103*, 41–50.
- (34) Hughes, M.; Morgan, H.; Flynn, M. J. *Colloid Interface Sci.* **1999**, *220*, 454–457.
- (35) Hughes, M. P.; Green, N. G. *J. Colloid Interface Sci.* **2002**, *250*, 266–268.
- (36) Ramos, A.; Morgan, H.; Castellanos, A. J. *Phys. D: Appl. Phys.* **1998**, *31*, 2338–2353.
- (37) Tran, S. L.; Cook, G. M. *J. Bacteriol.* **2005**, *187*, 5023–5028.
- (38) Basuray, S.; Chang, H.-C. *Phys. Rev. E* **2007**, *75*, 2–5.
- (39) Basuray, S.; Wei, H.-H.; Chang, H.-C. *Biomicrofluidics* **2010**, *4*, 022801.
- (40) Arnold, W. M.; Schwan, H. P.; Zimmermann, U. J. *Phys. Chem.* **1987**, *91*, 5093–5098.
- (41) Hughes, M.; Morgan, H.; Flynn, M. J. *Colloid Interface Sci.* **1999**, *220*, 454–457.
- (42) Lyklema, J.; Dukhin, S.; Shilov, V. J. *Electroanal. Chem.* **1983**, *143*, 1–21.
- (43) Springer, M.; Korteweg, A.; Lyklema, J. J. *Electroanal. Chem.* **1983**, *153*, 55–66.
- (44) Lyklema, J.; Springer, M.; Shilov, V.; Dukhin, S. J. *Electroanal. Chem.* **1986**, *198*, 19–26.
- (45) Verbelen, C.; Dupres, V.; Menozzi, F. D.; Raze, D.; Baulard, A. R.; Hols, P.; Dufrière, Y. F. *FEMS Microbiol. Lett.* **2006**, *264*, 192–197.
- (46) Nguyen, L.; Scherr, N.; Gatfield, J.; Walburger, A.; Pieters, J.; Thompson, C. J. *J. Bacteriol.* **2007**, *189*, 7896–7910.
- (47) Takade, A.; Umeda, A.; Matsuoka, M.; Yoshida, S.-i.; Nakamura, M.; Amako, K. *Cell* **2003**, *47*, 265–270.
- (48) Paul, T. R.; Beveridge, T. J. *J. Bacteriol.* **1992**, *174*, 6508–6517.
- (49) Paul, T. R.; Beveridge, T. J. *Infect. Immun.* **1994**, *62*, 1542–1550.
- (50) Paul, T. R.; Beveridge, T. J. *Zbl. Bakt.: Int. J. Med. Microbiol.* **1993**, *279*, 450–457.
- (51) Chan, K.; Gascoyne, P.; Becker, F.; Pethig, R. *Biochim. Biophys. Acta* **1997**, *1349*, 182–196.
- (52) Zhou, X.-F.; Markx, G. H.; Pethig, R.; Eastwood, I. M. *Biochim. Biophys. Acta* **1995**, *1245*, 85–93.
- (53) Arnold, W. M.; Schwan, H. P.; Zimmermann, U. J. *Phys. Chem.* **1987**, *91*, 5093–5098.
- (54) Gimsa, J. *Bioelectrochemistry* **2001**, *54*, 23–31.
- (55) Pethig, R.; Jakubek, L. M.; Sanger, R. H.; Heart, E.; Corson, E. D.; Smith, P. J. S. *IEE Proc. Nanobiotechnol.* **2005**, *152*, 189–193.
- (56) Hoettges, K. F.; Dale, J. W.; Hughes, M. P. *Phys. Med. Biol.* **2007**, *52*, 6001–6009.
- (57) Johari, J. H.; Bner, Y.; Hull, J. C.; Dale, J. W.; Hughes, M. P. *Phys. Med. Biol.* **2003**, *48*, N193–N198.